NJC

ROYAL SOCIETY OF CHEMISTRY

PAPER

View Article Online
View Journal | View Issue

Cite this: *New J. Chem.*, 2021, 45, 10488

Noticeable improvement in the toxic gas-sensing activity of the Zn-doped TiO_2 films for sensing devices

V. Gopala Krishnan,*[a] P. Elango,[b] K. Ravikumar,[c] R. Marnadu,[d] Omar M. Aldossary[e] and Mohd Ubaidullah *[f]

Received 5th March 2021,
Accepted 4th May 2021

DOI: 10.1039/d1nj01079d

rsc.li/njc

Zn-doped TiO_2 films were deposited on ultrasonically treated alumina substrates *via* the automatic nebulizer spray pyrolysis method. In this study, the thickness of the as-prepared films was gradually reduced, and their Brunauer–Emmett–Teller (BET) surface area and pore volume results were notably improved; in addition, values for the blue-shifted sharp edge absorption with an enlarged bandgap (E_g) were revealed in the deposited films. The agglomerated granular form has evolved into tiny grains with porous brighter particles scattered over the surface of the coated films. The sensing performance to reducing gases for combustible gas of ammonia (NH_3) and volatile organic compounds of methanol (CH_4O) and formaldehyde (HCHO) with the function of operating temperature and gas concentration were studied, and the highest sensing response of the hazardous formaldehyde (HCHO) reducing gas was noticed.

1. Introduction

In recent years, the amount of toxic and dangerous gases has been increasing dramatically due to the rapid technological impact on the medical, automotive, infrastructure and industrialization sectors, causing enormous outdoor and indoor pollution and numerous undesirable health effects.[1] Gas leak measurements play an important role in the area of nuclear power plants,[2] soil/wastewater treatment,[3] food and cosmetics,[4,5] and in the pharmaceutical industry[6] to monitor and alarm the dangerous gas levels. Toxic and dangerous matrices have been tested *via* calorimetric, conductive, gravimetric, optical, and numerous other sensing methods.[7] Of all, conductive metal oxide sensors are considered efficient due to their ability to operate at low humidity levels. Furthermore, they can detect environmental pollutant gases, including combustibles, because of the abundant adsorption of oxygen and the good catalytic effects.[8]

The most promising metal oxides sensors such as ZnO, WO_3, SnO_2, In_2O_3, and TiO_2 are used to detect combustible and volatile organic compounds (VOCs) as a function of change in resistance to the target gases.[9] Among them, TiO_2 and TiO_2-derived materials are significant for emerging environmental refinement.[10] TiO_2 has been extensively used in numerous applications such as a water treatment material, photocatalyst and gas sensor.[11–14] Despite numerous features, gas sensor-related parameters such as gas concentration, high operating temperature, sensor response, and selectivity are the main concerns that need to be improved. They can possibly be improved by doping the metal into metal oxides.[15] As with numerous combinational metal oxides, the metal-doped TiO_2 is a potential composition to improve the gas detection response, selectivity, stability, and even TiO_2 properties, such as Fermi level (E_f), electrical conductivity, and forbidden gap (E_g) value. Numerous studies have been devoted to the metal ion-doped TiO_2 gas detection such as Ag–TiO_2,[13] Sn–TiO_2, Nb–TiO_2 and Cr–TiO_2,[16] but no specific results are available for the stabilized anatase phase of additive mixed TiO_2 for the detection of combustible and volatile organic compounds. This report shows the characterization and gas sensing performance of anatase-phased Zn-doped TiO_2 for the combustible gas ammonia (NH_3), and volatile organic compounds methanol (CH_4O) and formaldehyde (HCHO) as the function of operating temperature and gas concentration.

[a] *Department of Physics, Dr N.G.P. Arts and Science College, Coimbatore - 641048, Tamil Nadu, India. E-mail: yuvagopal@yahoo.in*
[b] *Department of Physics, Government Arts College, Coimbatore - 641018, Tamil Nadu, India*
[c] *Department of Physics, Vivekanandha College of Arts and Science for Women, Tiruchengode-673205, Tamil Nadu, India*
[d] *Department of Physics, Sri Ramakrishna Mission Vidyalaya College of Arts and Science, Coimbatore-641 020, Tamil Nadu, India*
[e] *Department of Physics and Astronomy, College of Science, King Saud University, P. O. Box 2455, Riyadh 11451, Saudi Arabia*
[f] *Department of Chemistry, College of Science, King Saud University, Riyadh 11451, Saudi Arabia. E-mail: mtayyab@ksu.edu.sa*

2. Experimental

The automated nebulizer spray pyrolysis (ANSP) method was opted for preparing the microstructured Zn-doped TiO_2 films at 500 °C on the ultrasonically cleaned Al substrate; the details of the experimental procedure are specified in our earlier study.[17] Initially, 0.3 mole of titanium tetra-isopropoxide (TTIP) [$Ti[OCH(CH_3)_2]_4$] was dissolved into a 50 ml mixed solution of ethanol (EtOH) [C_2H_5OH] and acetylacetone (AcAc) [$CH_3COCH_2COCH_3$] in the ratio of 4 : 1 and constantly stirred for 30 min using a magnetic stirrer. Similarly, 0.3 mole of zinc acetate (ZnAc) [$Zn(CH_3COO)_2 \cdot 2H_2O$] was dissolved into 10 ml of ethanol and stirred for 30 mi. The stoichiometric volume percentages of $Zn_xTi_{1-x}O_2$ followed were X = 0.00%, 2.50%, 5.00%, 7.50% and 10.0%, and the mixer solution was filled out into the nebulizer container and sprayed on the 500 °C heated alumina substrate in the air atmosphere.

The characterization of the microstructured Zn-doped TiO_2 films was examined by the VSW instruments with Mg Kα (1253.6eV) and Al Kα (1486.6 eV) radiations; a Bruker D8 X-ray diffractometer with Cu Kα radiation (λ = 0.15418 nm) was used for the composition and structural analyses. SJ-301 Mitutoyo, Quanta-250 FEG with 30.0 kV, and the adsorption of Nitro nitrogen (N_2) with a micro-merit of 2700 micro-pulse pulses were used for the thickness, morphology and the BET surface analysis of the as-prepared films. The microscopic structure and the particle size were determined on a high-resolution transmission electron microscope (HRTEM) Jeol/JEM 2100 with SAED using 200 kV. For the optical study, the JASCO-V-570 model was used with a 250–970 nm UV-Vis spectrophotometer. The LCR GW Instek LCR-821 bridge model (0.01 kΩ to 100 MΩ) was used to analyze gas detection performance.

3. Result and discussion

The X-ray photoelectron spectroscopy (XPS) elemental analysis of the narrow and broad emission spectra of Zn-doped TiO_2 is shown in Fig. 1(a–f). It is clearly seen that both undoped and Zn-doped TiO_2 matrices have no XPS signals from other impurities except O 2s, 1s (1/2), C 1s, Zn 2p (3/2, 1/2) and Ti 3p, 2p (3/2, 1/2) sites. The presence of C 1s element was due to sample handling and reference part of this survey scan. In addition, the intensity variation between undoped and Zn-doped TiO_2 shows the inadequate crystallization and ionic radius difference for Zn^{2+} and Ti^{4+} about 0.74 Å and 0.605 Å, respectively. The valence band sites of 23.1 eV and 38 eV are attributed to O 2s and Ti 3p peaks, respectively. The parent metal (Ti 2p) shows two spin orbit doublets, which correspond to the core level of Ti^{4+} 2p (3/2 and 1/2) assigned to 459.5 eV and 465.2 eV, respectively.[18] The additive metal of Zn also shows the two spin orbit doublets for Zn 2p (3/2 and 1/2) are assigned to 1022.6 eV and 1045.7 eV binding energies, respectively, and the difference between these two peaks is 23.1 eV, which denotes that the surface of $Zn_{0.05}Ti_{0.95}O_2$ is combined with the oxygen bond and Zn^{2+} site.[19] Finally, the XPS peak at 530.9 eV can be attributed to the O-Ti bonds of the O $1s_{1/2}$ oxygen state. The stabilized anatase-phase Ti^{4+} was well-fitted with the undoped and Zn-doped TiO_2 microstructured films, and their atomic weight percentages are represented in Table 1.

The X-ray diffraction (XRD) patterns of the microstructured Zn-doped TiO_2 films are depicted in Fig. 1(g). The anatase-phased polycrystalline tetragonal structure reflected plane orientation has been indexed to (101), (004), (200), (105) and (204) corresponding to $2\theta^\circ$ = 25.39, 38.04, 48.14, 54.01 and 62.91 angles, well-fitted with standard JCPDS card no. 89-4921.

The XRD spectrum was not detected for the rutile and brookite phases of TiO_2 due to the stabilization of the as-prepared films obtained by raw materials and preparation method.[20] The doping of the Zn metal ion increased with the decrease in the parent metal oxide (TiO_2) dominant phase intensity, and also, a few reflected plane orientations corresponding to (200), (105), (211) and (204) have been disappeared. In addition, the dominant peak of the Zn metal ion (002) reflected plane orientation corresponds to $2\theta^\circ$ = 34.41°, specified as (*) at a higher concentration (*i.e.*, 7.50% and 10.0%) and further doping could disperse the anatase-phased TiO_2 crystallization, indicating that Zn^{2+} was introduced into the anatase-phase matrix to form a solid-solution $Zn_xTi_{1-x}O_2$ because of the ionic radius between Zn (0.74 Å) and Ti (0.605 Å), respectively.[21] Particularly, Fig. 1(h) has shown the intensity variation of the limited angle and is the dominant peak of the TiO_2 anatase-phase crystal structure. The specified dominant peak (101) has been gradually varied, and their angle was shifted to a shorter angle due to the doping of the Zn metal ion. The calculated lattice plane values are a = 3.780 Å and c = 9.519 Å, which show that the unit cell parameter may be reformed a little with standards Ti^{4+} data. Their average particle size was calculated using the Scherrer formula,[22] and the obtained particle sizes are represented in Table 1. The thickness of the as-prepared films gradually decreased with the increase in the Zn metal ion concentration (Table 1), similar to the XRD particle size value. The BET (Brunauer–Emmett–Teller) method was used to analyze the BET surface area, total pore volume and average pore diameter of the Zn-doped TiO_2 microstructured samples, and the results are presented in Table 1. The results indicate that the microstructured Zn-doped TiO_2 surface area and pore volume gradually increased, and their average pore diameter drastically reduced with an increase in the Zn metal ion concentration. This result shows that the good sensing response can be obtained from higher concentration to lower concentration of Zn metal ions. This is because the higher surface area of the sample enables to raise the interface between the sensor material and gas molecules.[23]

The optical study results of the microstructured Zn-doped TiO_2 films are shown in Fig. 1(i–j). The oscillating nature of transmittance has been observed from the as-prepared samples, and the least transmittance for undoped TiO_2 can be improved by doping Zn metal into TiO_2. A higher transmittance (49.94%) was observed at 570 nm by increasing the Zn metal ion concentration. In addition, the observed transmittance spectrum shows a sharp absorption edge between 359 nm and 317 nm in the ultraviolet

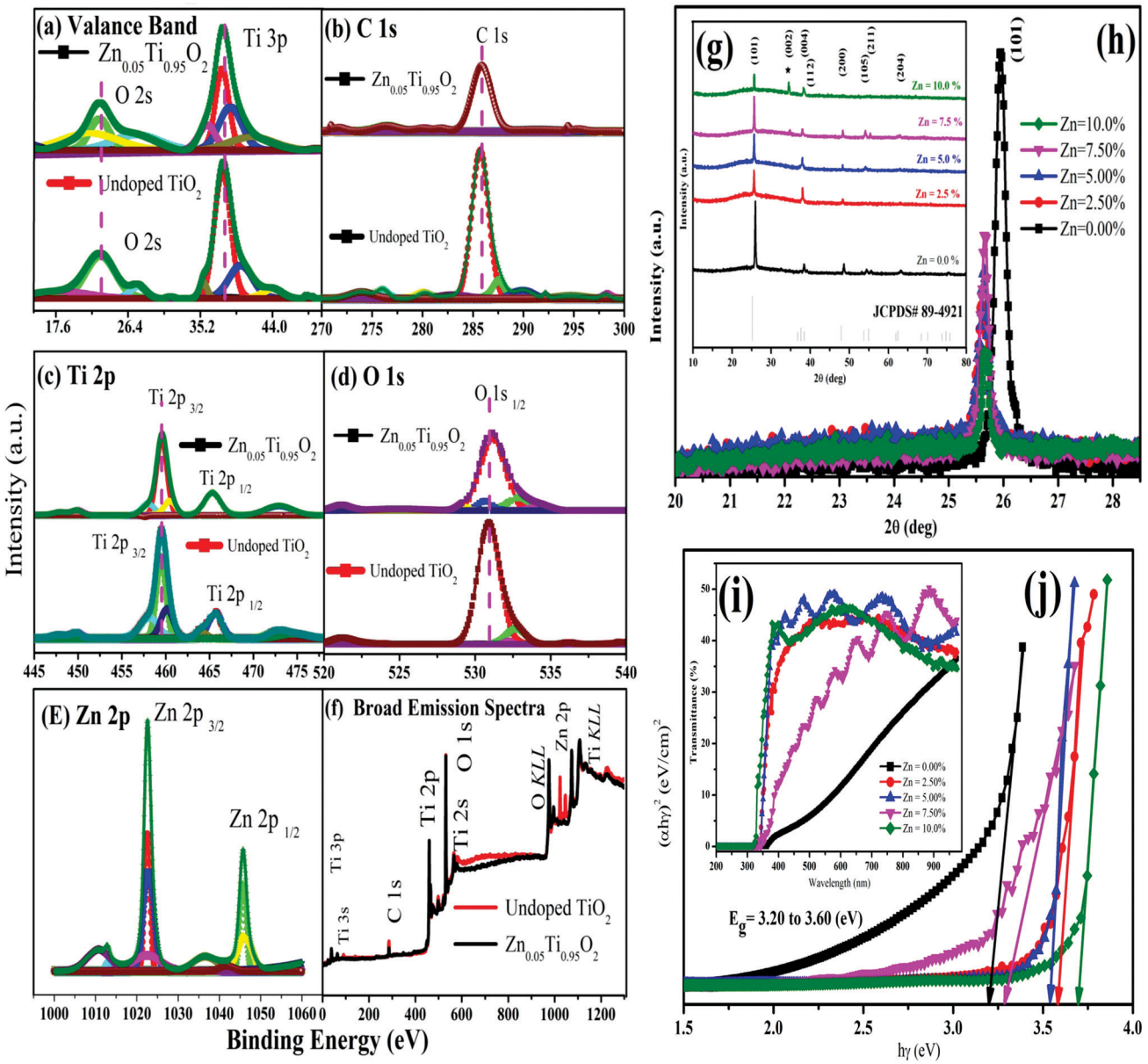

Fig. 1 (a–f) Compositional analysis of the XPS study for Zn-doped TiO_2 films, (g–h) X-ray study and intensity variation of the limited angle, (i–j) transmittance and band representation of the optical study.

range, which reveals the blue shift, due to the reduction of porosity and unfair crystalline structure,[21] and as a rule, <400 nm optical absorption can be ascribed to the electron conversions from the valence band to the conduction band.[24] Moreover, the bandgap (E_g) value has been calculated using the Tauc's relation.[25] The bandgap value increased from 3.20 eV to 3.60 eV with the increase in the Zn concentration, while the bandgap value of anatase-phased Ti^{4+} exactly coincided (*i.e.*, Zn = 0.00%). The Zn dopant can improve the interfacial coupling effect and adsorption ability to the parent metal oxide (TiO_2), elevating the bandgap value from a lower to higher level.[24] Usually, broad bandgap (~3.60 eV) metal oxides are the potential candidate for gas sensing materials on account of their strange electrical behavior and excellent stability.

The surface morphological study results obtained using a field emission scanning electron microscopy (FESEM) are shown in Fig. 2(a–e), which exhibit the agglomerated granular shape for undoped TiO_2 (Zn = 0.00%); the doping of Zn metal ions into TiO_2 shows the tightly packed tiny grains (Zn = 2.50%), and later, segregated tiny grains were observed at Zn = 5.00%. Further, the doping of Zn metal ions into TiO_2 (*i.e.*, 7.50% and 10.0%) revealed that the segregated tiny grains with porous brighter particles were scattered on the surface of the as-prepared films and their morphology changes to a porous hexagonal crystal structure due to the ionic radius difference between Zn^{2+} and Ti^{4+} ions. The observed FESEM result shows that the appropriate particle size and rough porous surface of Zn-doped TiO_2 enhances the gas adsorption

Table 1 Elemental analysis of the XPS study, structural characterization and BET analysis of the Zn-doped TiO_2 microstructured films

X-Ray photoelectron spectroscopy		
Elements	(Zn = 0. 00%) (at%)	(Zn = 5.00%) (at%)
Ti 2p	27.66	19.33
Zn 2p	—	1.18
O 1s	58.21	47.12
C 1s	14.13	32.37

Structural and surface characterization of Zn-doped TiO_2					
Zn %	Avg. particle size (nm)	Thickness (nm)	BET surface area ($m^2\ g^{-1}$)	Total pore volume ($cm^3\ g^{-1}$)	Avg. pore diameter (Å)
0.00	48.20	493	132	0.39	102
2.50	43.85	472	319	0.61	78
5.00	41.28	412	387	0.68	63
7.50	44.60	381	431	0.72	59
10.0	37.03	296	493	0.77	54

behavior and also confirms the results of the XRD study. In addition, inset Fig. 2(e1) shows the high-resolution transmission electron microscopy (HRTEM) structure, and it was confirmed that the microparticles were scattered over the surface within the range of 20 nm. Furthermore, the selected area electron diffraction (SAED) pattern shown as inset Fig. 2(e2) confirmed the prominent anatase phase of TiO_2.

Gas sensing performance

TiO_2 metal oxides allow the electrical resistance to be modified when exposed to oxidizing and reducing gases. The n-type semiconducting TiO_2 metal oxide shows the increasing resistance to oxidizing gases, while decreasing resistance to reducing gases.[26] Additive metal ions overcome the drawback of the metal oxide sensor and supply excess of negative electron charge carriers (n-type) and improve the gas detection performance of the parent metal oxide (TiO_2) sensor material.[27] Among all, Zn-doped TiO_2 oxide offered non-transformation phase (only anatase), large surface area, strange electrical behavior, superior gas adsorption and excellent stability towards the sensor material, termed as chemoresistor. The chemoresistor material could vary its electrical resistance in response to changes in the chemical atmosphere. A basic chemoresistor is made up of a sensitive material that closes the gap between two electrodes, which can easily measure the resistance between the electrodes. The sensor material has an intrinsic resistance that can be modulated in the presence of the target gas. During exposure, the target gas interacts with the sensing material, causing a change in the resistance reading.[28] The chemoresistor performance for combustible gas ammonia (NH_3) and volatile organic compounds methanol (CH_4O) and formaldehyde (HCHO) with the function of operating temperature and gas concentration has been investigated, and the sensor device details are represented in our early work.[25] In general, the chemoresistor forms a chemisorbed oxygen species (O^-, O_2^-, and O^{2-}) and generates numerous free electrons on the sensor surface due to the exposure of reducing gases on account of increasing the gas sensing response.[21]

Fig. 2(f–h) shows the resistance mode response of NH_3, CH_4O and HCHO reducing gases towards the Zn-doped TiO_2 sensor material (chemoresistor) at 150 °C operating temperature and 100 ppm gas concentration. The resistance value in the range of 10–70 MΩ was observed, and the HCHO reducing gas shows drastic reduction response towards resistance as that of all remaining reducing gas (NH_3 and CH_4O). Moreover, the inset in Fig. 2(i–k) shows the gas sensing response towards numerous Zn concentrations (0.00% to 10.0%, in step of 2.50%) of the chemoresistor, which clearly revealed that the Zn concentration increased with an increase in the gas sensing response at 150 °C operating temperature and 100 ppm gas concentration. Fig. 2(l) shows the bar chart of selective response to reducing gases (NH_3, CH_4O and HCHO) as a function of the operating temperature at 150 °C with 100 ppm gas concentration, depicting the maximum response to formaldehyde (HCHO) reducing gas to Zn = 10.0% concentration of the chemoresistor and minimum response to methanol (CH_4O) reducing gas to the Zn = 0.00% concentration (TiO_2) chemoresistor and the moderate response to ammonia (NH_3) reducing gas to the Zn-doped TiO_2 chemoresistor.

In the gas sensing mechanism, the operating temperature (°C) and gas concentration (ppm) play major roles in influencing the reducing gases to generate the chemisorbed oxygen species (O^-, O_2^-, O^{2-}) with a free negative charge carrier on the chemoresistor. Fig. 2(m) shows the gas response as the function of gas concentration (ppm) for the HCHO reducing gas at 150 °C operating temperature. The gas concentration level 40–200 ppm was noted. The gas concentration increased with the increase in the gas response up to 100 ppm, and subsequently decreased with the increase in the gas concentration due to the surface adsorption between oxygen species and reducing gases.[29] Similarly, the Zn-doped TiO_2 chemoresistor shows a linear behavior, and the Zn concentration (0.00% to 10.0%, in step of 2.50) chemoresistor exhibits minimum to maximum sensing response, respectively. The operating temperature range from 50 °C to 300 °C with the relation of the constant gas concentration (100 ppm) to HCHO reducing gas is shown in the inset in Fig. 2(n). From this observation, the operating temperature and Zn concentration increased with the increase in the gas sensing response up to 100 °C, after which it decreased with the increase in the operating temperature. Because of which, the adsorption energy and the activation energy (E_a) have been improved up to an optimal operating temperature (*i.e.*, 150 °C). Then, desorption and Schottky barrier heights were gradually raised to decrease the sensing response of the chemoresistor.[20]

Fig. 2(o) shows the cyclical response towards the HCHO reducing gas at an optimal temperature of 150 °C with the surface adsorbed level of gas concentration (100 ppm). The cyclic gas response towards the Zn-doped TiO_2 chemoresistor increased with the increase in the Zn concentration, and the linear response has been observed up to 5000 sec (~1.40 h) at repeated cycles. Moreover, the Zn concentration of 10.0%

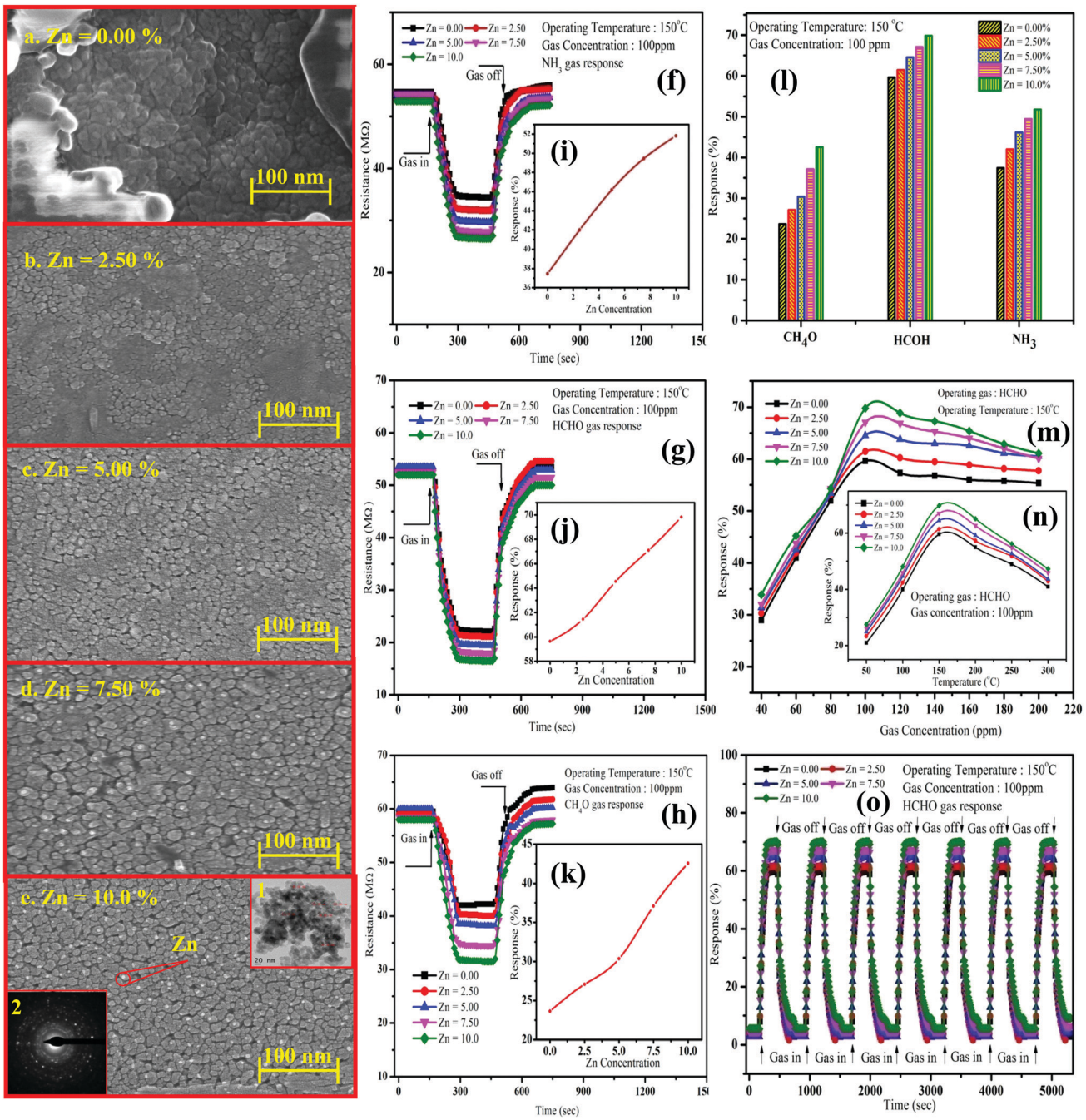

Fig. 2 (a–e) FESEM analysis and the inset of e (1, 2) shows the TEM image and the SAED pattern corresponding to Zn-doped TiO_2 films, (f–o) numerous aspects (resistance, selectivity, temperature, gas concentration, and cyclical response) of the gas sensing survey.

shows the highest sensing response compared to other Zn concentrations due to the spillover effects between oxygen species and reducing gas along with Zn concentration.[30] Present study of the Zn-doped TiO_2 chemoresistor shows the maximum response (~69.74%) towards the formaldehyde (HCHO) reducing gas. Formaldehyde (HCHO), a hazardous VOC, is found in numerous food products and causes severe health issues even at a low concentration.[31,32] Table 2 summarizes the gas response of the present study and reported study pertaining to the HCHO reducing gas.

The microstructured Zn-doped TiO_2 chemoresistor shows enhanced electrical property, surface area and gas adsorption catalysts of the chemoresistor, and their schematic sensing mechanism with the sensor material details are described in Fig. 3.

HCHO vapor is absorbed at the edges of the surface grain and reacts with the adsorbed oxygen species on the surface. The chemoresistor forms a type of chemisorbed oxygen (O^-, O_2^-, and O^{2-}) and traps the free electron by the chemical reaction between the surface depletion layer and

Table 2 Comparison of the HCHO sensing response to the present and reported values of the Zn-doped TiO_2 microstructured films

Materials	Parameter (Temp, Gas Conc.)	Sensing value (%)	Ref.
$ZnTiO_2$	150 °C/100 ppm	69.74	Present work
$NiO/NiFe_2O_4$	240 °C/100 ppm	22.5	10
TiO_2/SnO_2	360 °C/200 ppm	56.2	22
SnO_2 microspheres	200 °C/100 ppm	38.3	25
SnO_2–In_2O_3–CdO	133 °C/100 ppm	22.7	27
Cd-doped TiO_2-SnO_2	310 °C/100 ppm	15	28
Y-doped SnO_2	180 °C/50 ppm	18	29
$(Ti,Sn)O_2$ solid solution	350 °C/300 ppm	29.3	30

the microstructured grains.[33,34] It clearly describes that the surface density of the negatively charged oxygen species reacts with HCHO vapor adsorption, and the result is that the height of the Schottky barrier at the micro-gain limit has gradually decreased with the decrease in the barrier height of the sensor resistance. It has been synthesized to form a heterojunction (*n*-oxide-*n*-oxide) from Zn-doped TiO_2 metal oxide when the composition is exposed to the HCHO reducing gas. The gas molecules will react within the past adsorbed chemisorbed oxygen species in the chemoresistor surface, and the chemical performance is as represented in Fig. (3). Moreover, Fig. 3(b) shows the stability, response and recovery time of the HCHO reducing gas at 150 °C optimal temperature and surface adsorbed 100 ppm gas concentration. The stability of the chemoresistor was measured for 30 days after the initial measurement. The average response stability of the chemoresistor is ~69.74%, which shows good ageing capacity, reduced inner stress and even distributed particles. In addition, the response and recovery times of the chemoresistor were 40 s and 70 s, respectively. The fast response and slow recovery exposed their reduction and oxidizing mechanisms.

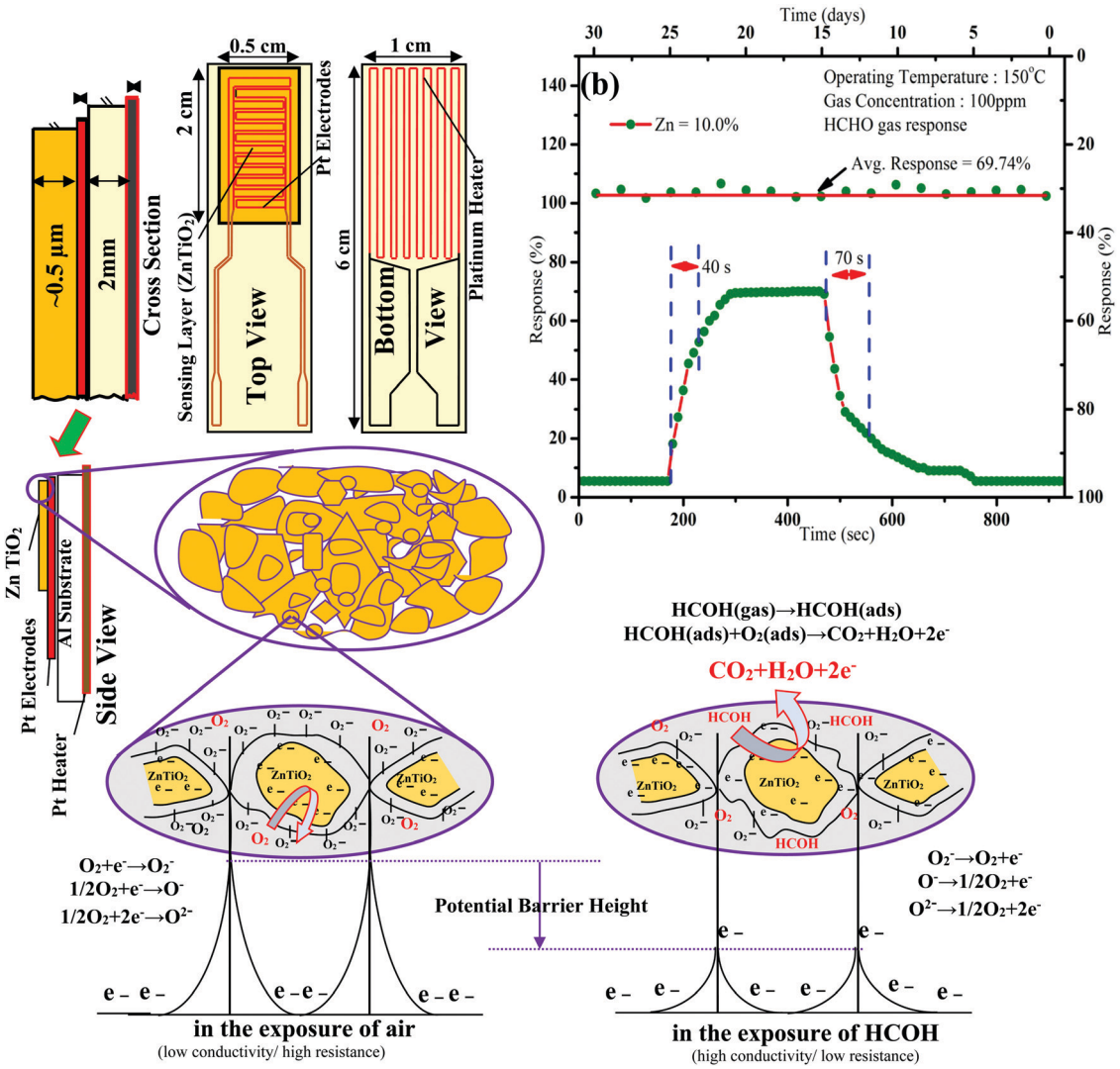

Fig. 3 Sensing element view, sensing mechanism, stability, response and recovery time of the Zn-doped TiO_2 films.

4. Conclusions

The divalent (Zn^{2+}) metal ions were successfully doped into the tetravalent (Ti^{4+}) metal ion, and the composition was deposited on the alumina substrate using an automated nebulizer spray pyrolysis method. From all the study discussed, the XPS study has shown the relevant chemical composite doping to metal-doped metal oxide. The XRD study shows only the anatase-phase polycrystalline tetragonal structure with a reduced particle size and intensity varied dominant peaks were observed by increasing the Zn concentration. The microstructured film thicknesses and average pore diameter were decreased, and the surface area and the pore volume were increased by increasing the Zn concentration. Better oscillating nature transmittance with blue-shift sharp absorption shows the bandgap value between 3.20 eV and 3.60 eV through the optical study. The surface morphology depicts the influence of the Zn metal concentration on TiO_2 metal oxide and also shows segregated tiny grains with porous brighter particles scattered on the surface of the coated films. Zn-doped TiO_2 metal oxide revealed the better sensing behavior towards formaldehyde (HCHO) reducing gas at 150 °C operating temperature with 100 ppm gas concentration. Compared to the undoped TiO_2 chemoresistor, the Zn-doped TiO_2 chemoresistor creates the modification in electrical property, gas adsorption, surface area and surface morphology. The developed Zn-doped TiO_2 metal oxide composite detects formaldehyde (HCHO) more sensitively, which in turn helps humans to protect from health issues.

Conflicts of interest

None to declare.

Acknowledgements

The authors extend their sincere appreciation to the Researchers supporting project number (RSP-2020/61), King Saud University, Riyadh, Saudi Arabia, for the financial support.

References

1 A. Mirzaei and J.-H. Lee, *et al.*, Resistive gas sensors based on metal-oxide nanowires, *J. Appl. Phys.*, 2019, **126**, 241102.
2 Y. Zhao and C. Smidts, A control-theoretic approach to detecting and distinguishing replay attacks from other anomalies in nuclear power plants, *Prog. Nucl.*, 2020, **123**, 103315.
3 J. Guilera and T. Andreu, *et al.*, Synthetic natural gas production from biogas in a waste water treatment plant, *Renewable Energy*, 2020, **146**, 1301.
4 T. R. Pavase and H. Lin, *et al.*, Recent advances of conjugated polymer (CP) nanocomposite-based chemical sensors and their applications in food spoilage detection: A comprehensive review, *Sens. Actuators, B*, 2018, **27310**, 1113.
5 A. R. García-Cicourel and H.-G. Janssen, Direct analysis of aromatic hydrocarbons in purified mineral oils for foods and cosmetics applications using gas chromatography with vacuum ultraviolet detection, *J. Chromatogr. A*, 2019, **159012**, 113.
6 K. Y. Hwa and P. Karuppaiah, *et al.*, Ultrasonic synthesis of CuO nanoflakes: A robust electrochemical scaffold for the sensitive detection of phenolic hazard in water and pharmaceutical samples, *Ultrason. Sonochem.*, 2019, **58**, 104649.
7 A. H. Khoshaman and B. Bahreyni, Application of metal organic framework crystals for sensing of volatile organic gases, *Sens. Actuators, B*, 2012, **162**, 114.
8 A. Berna, Metal oxide sensors for electronic noses and their application to food analysis, *Sensors*, 2010, **10**, 3882.
9 M. Batzill and U. Diebold, The surface and materials science of tin oxide, *Prog. Surf. Sci.*, 2005, **79**, 47.
10 D. Aphairaj and T. Wirunmongkol, *et al.*, Effect of calcination temperatures on structures of TiO_2 powders prepared by hydrothermal method using Thai leucoxene mineral, *Energy Procedia*, 2011, **9**, 539–544.
11 B. Banerjee and A. Bhaumika, *et al.*, Green synthesis of Pt-doped TiO_2 nanocrystals with exposed (001) facets and mesoscopic void space for photo-splitting of water under solar irradiation, *Nanoscale*, 2015, **7**, 10504–10512.
12 P. Mondal and A. Bhaumik, *et al.*, Palladium nanoparticles embedded on mesoporous TiO_2 material (Pd@MTiO$_2$) as an efficient heterogeneous catalyst for Suzuki-Coupling reactions in water medium, *J. Colloid Interface Sci.*, 2017, **508**, 378–386.
13 H. Liu and W. Shen, A room temperature operated ammonia gas sensor based on Ag-decorated TiO_2 quantum dot clusters, *RSC Adv.*, 2019, **9**, 24519.
14 S. Ngamsinlapasathian and T. Sreethawong, *et al.*, Single- and double-alayered mesoporous TiO_2/P25 TiO_2 electrode for dye-sensitized solar cell, *Energy Mater. Sol. Cells*, 2005, **86**, 269.
15 Y. Xu and X. Tian, formaldehyde gas sensor with improved gas response and sub-ppm level detection limit based on NiO/$NiFe_2O_4$ composite nanotetrahedrons, *Sens. Actuators, B*, 2020, **309**, 127719.
16 K. Zakrzewska and M. Radecka, Effect of Nb, Cr, Sn additions on gas sensing properties of TiO_2 thin Films, *Thin Solid Films*, 1997, **310**, 161.
17 V. Gopala Krishnan and P. Elango, pH deeds on structural, optical, electrical and gas sensing performance of TiO_2 nanofilms by automated nebulizer spray pyrolysis technique, *Optik*, 2016, **127**, 11102.
18 Y. Zhao, C. Li, X. Liu, F. Gu, H. L. Du and L. Shi, Zn-doped TiO_2 nanoparticles with high photocatalytic activity synthesized by hydrogeneoxygen diffusion flame, *Appl. Catal., B*, 2008, **79**, 208.
19 H. Fei and Y. Li, Zinc pyridinedicarboxylate micro-nanostructures: promising anode materials for lithium-ion batteries with excellent cycling performance, *J. Colloid Interface Sci.*, 2016, **481**, 256.

20 V. Gopala Krishnan and A. Purushothaman, Effect of thickness on the physical properties and gas sensing application: anatase titanium dioxide nanofilms by automated nebulizer spray pyrolysis (ANSP), *J. Mater. Sci.: Mater. Electron.*, 2017, **28**, 11473.
21 V. Gopala Krishnan and P. Elango, Automated nebulizer sprayed tin doped titanium dioxide ($Sn_xTi_{1-x}O_2$) anatase nanofilms properties, gas sensing performance, *Mater. Chem. Phys.*, 2017, **199**, 113.
22 C. Sankar and V. Ponnuswamy, Structural, morphological, optical and gas sensing properties of pureand Ru doped SnO_2 thin films by nebulizer spray pyrolysis technique, *Appl. Surf. Sci.*, 2015, **349**, 931.
23 M. S. Hosseini and S. Zeinali, Fabrication of capacitive sensor based on Cu-BTC (MOF-199) nanoporous film for detection of ethanol and methanol vapors, *Sens. Actuators, B*, 2016, **230**, 9.
24 Y. Zhao and C. Li, *et al*., Zn-doped TiO_2 nanoparticles with high photocatalytic activity synthesized by hydrogen–oxygen diffusion flame, *Appl. Catal., B*, 2008, **79**, 208.
25 V. Gopala Krishnan and P. Elango, Surface characterization and gas sensing performance of yttrium doped TiO_2 nanofilms prepared by automated nebulizer spray pyrolysis (ANSP), *J. Mater. Sci.: Mater. Electron.*, 2018, **29**, 392.
26 W. Zeng and T. Liu, Sensitivity improvement of TiO_2-doped SnO_2 to volatile organic compounds, *Phys. E*, 2010, **43**, 633.
27 G. Eranna, *Metal oxide nanostructures as gas sensing devices*, CRC Press, Boca Raton, FL, USA, 2012.
28 W. Hu and L. Wan, *et al.*, Electronic noses: from advanced materials to sensors aided with data processing, *Adv. Mater. Technol.*, 2019, **4**, 1800488.
29 Y. Lia and N. Chen, Formaldehyde detection: SnO_2 microspheres for formaldehyde gassensor with high sensitivity, fast response/recovery and goodselectivity, *Sens. Actuators, B*, 2017, **238**, 264.
30 L. A. Patil and D. N. Suryawanshi, *et al.*, Pt doped TiO_2 thin films prepared by spray pyrolysis for hydrogen gas detection, *Bull. Mater. Sci.*, 2014, **37**(3), 425.
31 T. Chen and Q. J. Liu, A high sensitivity gas sensor for formaldehyde based on CdO and In_2O_3 doped nanocrystalline SnO_2, *Nanotechnology*, 2008, **19**, 095506.
32 W. Zeng, T. Liu, Z. Wang, S. Tsukimoto, M. Saito and Y. Ikuhara, Selective detection of formaldehyde gas using a Cd-doped TiO_2-SnO_2 sensor, *Sensors*, 2009, **9**(11), 9029.
33 K. Zhu and S. Ma, Highly sensitive formaldehyde gas sensors based on Y-doped SnO_2 hierarchical flower-shaped nanostructures, *J. Alloys Compd.*, 2019, **792**, 938.
34 W. Zeng and B. Miao, Effect of Ti on the gas sensing characteristic of ($Ti_{0.5}Sn_{0.5}$) O_2 solid solutions, *Phys. E*, 2012, **44**, 2143.